Electronic Supplementary Material (ESI) for Physical Chemistry Chemical Physics.

Supporting Information

Revealing the reason for the reversal of properties from fullerene to nonfullerene

Jiu-Chang Huang, Ming-Yang Li, Li-Na Wu, Chun-Ni Xiao, Guang-Yan Sun*

Contents

S1 Materials and methods

Models

Based on five-membered ring and six-membered ring of C60, cutting C60 layer by layer respectively, establish two types of bowl-nonfullerene models. According to the base of ring, the bowl-nonfullerenes were divided into 5-ring model and 6-ring model, shown in **Figure S1**. As shown in **Figure 1**, bowl-nonfullerenes have π-conjugated and curved structure similar to C60. Pentacene (P) is chosen as the donor, which is often used in mechanism research. The initial configuration was built by Face-on stacking and a distance of 3.5 Å allowed the aromatic ring of acceptor to accurately stack on benzene ring in the middle of pentacene. Likewise for donor/acceptor (D/A) dimers, there are Face-on 5 and Face-on 6 to distinguish the initial stacking ring above the pentacene (**Figure S2**). All variables except the aromatic ring above the pentacene are controlled here.

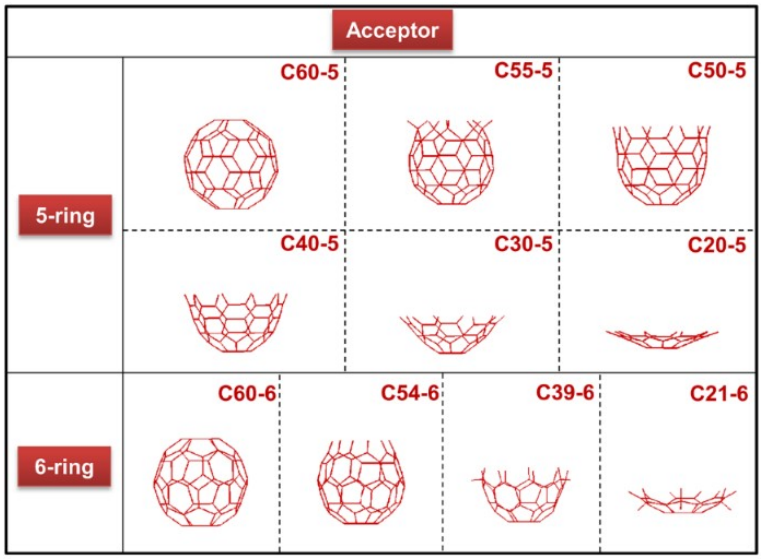

Figure S1. Bowl-nonfullerene molecules with 5-membered ring as base (5-ring model) and 6-membered ring as base (6-ring model).

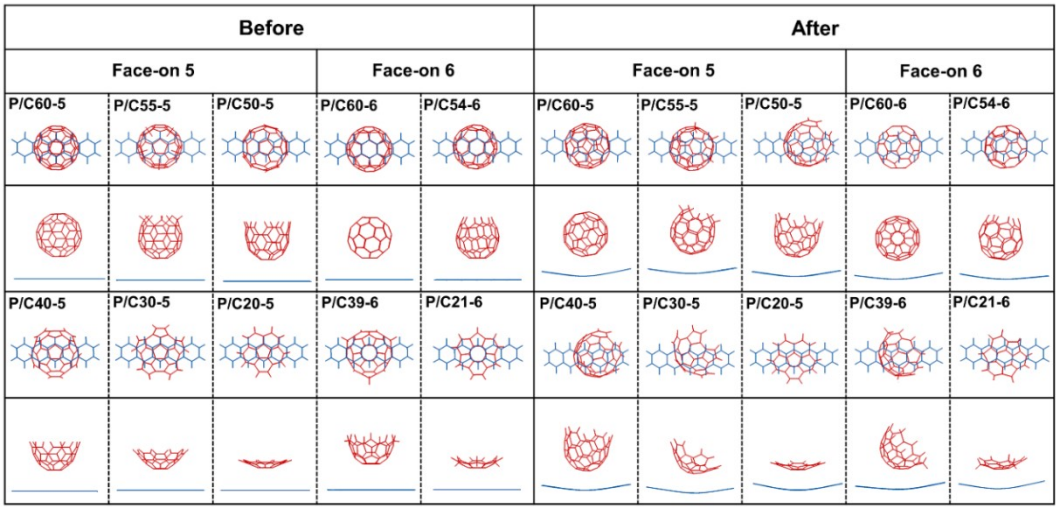

Figure S2. The configuration of each dimer before and after optimization in the Face-on 5 models and Face-on 6 models.

Methods

Since B3LYP has been certified reasonably to describe geometries and electronic structures well.[1,2] For 5-ring and 6-ring models, the geometry structure and excited state characteristic were carried out at the B3LYP/6-31G(d) level.[3] For Face-on 5 and Face-on 6 dimers, considering long-range coulomb interactions, ωB97XD is more conducive to describe the degree of delocalization of the wave function along with the intermolecular interaction.[4] Therefore, geometric optimization and excited-state calculations were performed at the ωB97XD/6-31G(d) level.[5] The range separation parameter ω depends on the size and conjugation degree of the system and it can be optimized as a function minimizer.[6]

$$\frac{1}{r}=\frac{erf(\omega r)}{r}+\frac{erfc(\omega r)}{r} \quad \text{.....(1)}$$

The first item on the right side of the equal sign is the short-range description obtained by the semilocal/hybrid DFT method, and the second item involves long-range description obtained by combining DFT for correlation and Hartree-Fock for exchange. Our calculation about optimized ω was conducted using the optDFTω code.[7] All calculations mentioned above were performed in the Gaussian09 software package.[8] In addition, the characterization methods in the results and discussions are obtained from Multiwfn 3.7.[9]

Table S1. The optimal ω value for each system

Model	ω (Bohr^{-1})	Model	ω (Bohr^{-1})
P/C60-5	0.1373	P/C20-5	0.1439
P/C55-5	0.1227	P/C60-6	0.1391
P/C50-5	0.1235	P/C54-6	0.1364
P/C40-5	0.1367	P/C39-6	0.1308
P/C30-5	0.1351	P/C21-6	0.1419

S2 Influencing factors before and after the dominant energy level change

As we all know, the difference in symmetry leads to a larger difference in energy level, which is transmitted through electronic changes. Furthermore, by cutting the number of electrons, the shielding of the attractive potential of the nucleus is weakened, and the energy is reduced accordingly. To this end, we need to integrate the distribution of the electron clouds on the orbitals, the number of electrons, the ability of giving (HOMO) and withdrawing (LUMO) electrons and the symmetry to consider the causes and influencing factors of inflection point appearing from C60 to the smallest unit (C20-5 and C21-6). As shown in **Figure S4**, for the 5-ring model, smaller changes from C60 to C55-5 do not cause major changes in the distribution of electron clouds and number of electrons. So the increase of energy level mainly comes from the breaking of symmetry. From C55-5 to C50-5, they have similar electron clouds distribution, where electrons are enriched at the bottom and outside of ring. And the symmetry of C55-5 and C50-5 is similar, so the energy level reduction is caused by a slight change in the number of electrons. From C50-5 to C40-5, due to a decrease in the number of electrons, the LUMO energy level shows a decreasing trend.

However, from C40-5 to C30-5 and C30-5 to C20-5, the substantial decrease in the number of electrons could not bring a decrease in the LUMO energy level, but an increase. It shows that symmetry dominates the energy change in the two gradient changes. The reason for C40-5 as inflection point is that the factors before and after the dominant energy level change from number of electrons to symmetry. For the 6-ring model, C60 to C54-6, like C60 to C55-5, the decrease in symmetry increases the LUMO energy level slightly. From C54-6 to C39-6, there is a major difference in the distribution of the electron clouds, where electron enrichment from the outside of the ring to the whole molecule, eventually leading to an increase in energy level. C39-6 to C21-6 is also similar to C30-5 to C20-5, which are affected by symmetry. The reason for C54-6 as inflection point is that the factors before and after the dominant energy level change from symmetry to the distribution of the electron clouds. In a word, although the electronic transition form of HOMO→LUMO is π→π*, the energy level degeneracy is different due to the difference in the transition trajectory, and this is due to the small difference in structure from fullerene to bowl-fullerene.

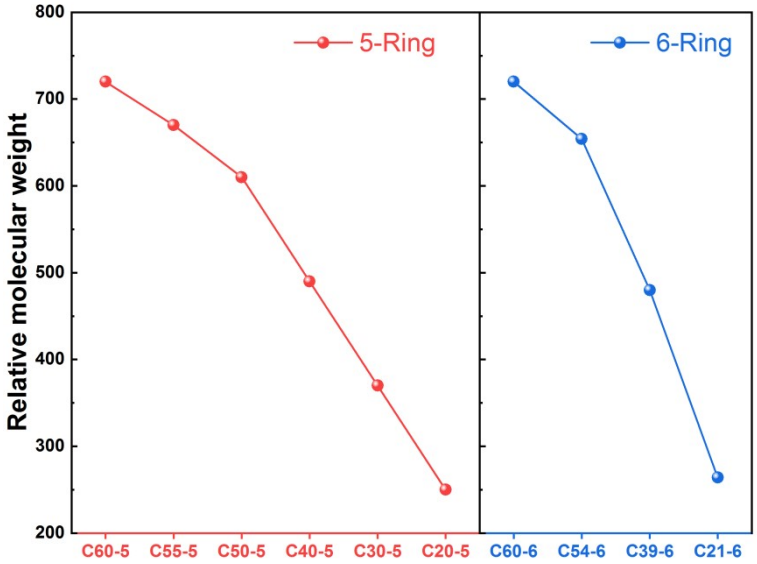

Figure S3. The changing trend of relative molecular weight of the model molecules.

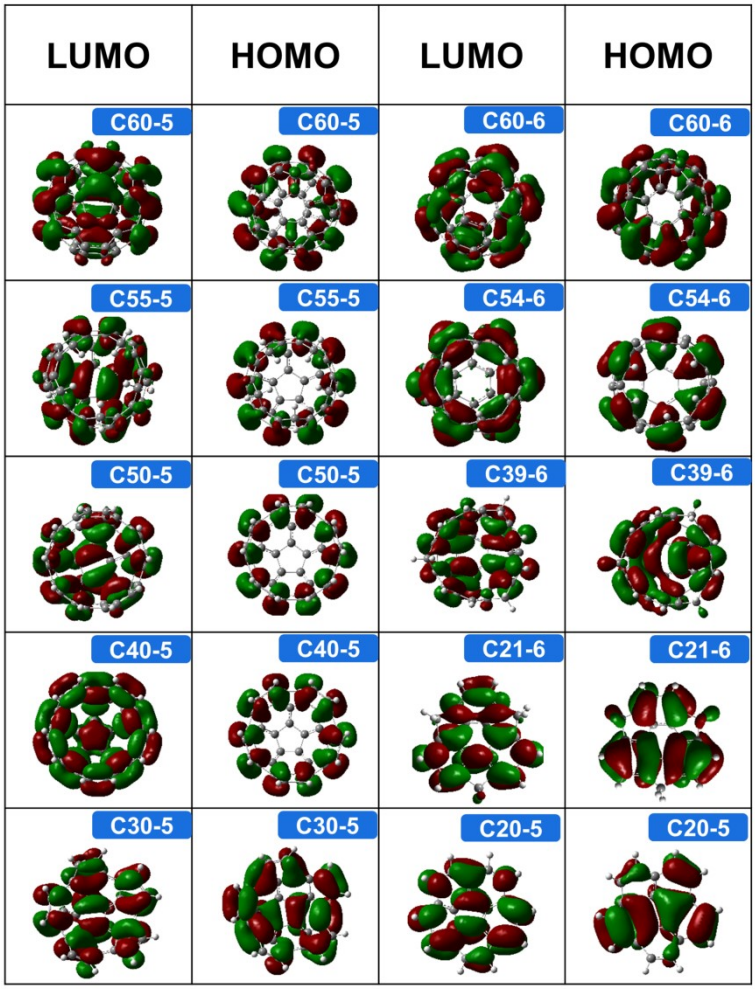

Figure S4. Frontier molecular orbital diagrams of fullerene and bowl-nonfullerene models (including 5-ring and 6-ring model).

S3 Supplement of Results

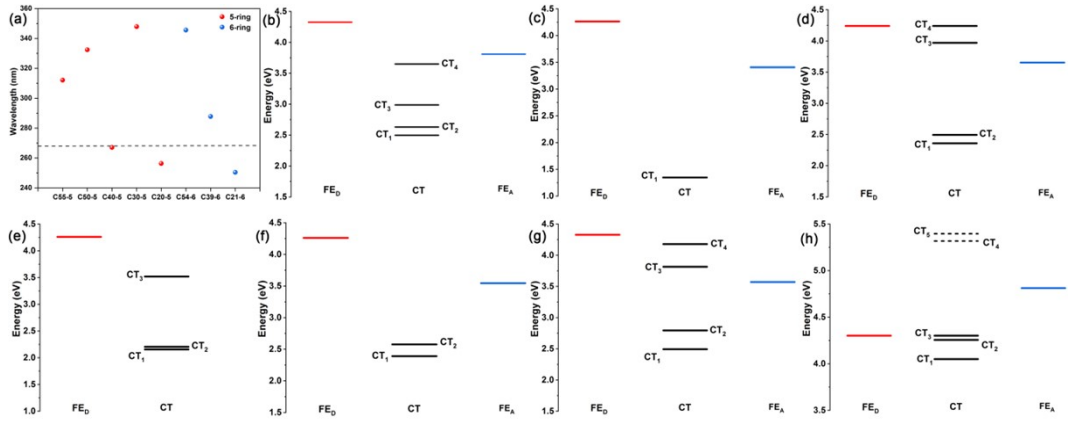

Figure S5. (a) The maximum absorption wavelength (λ_{max}) of bowl-nonfullerene, the dotted line denotes the λ_{max} of pentacene. (b-h) Excitation energies (eV) of Frenkel excitons and the CT states of (b) P/C55-5, (c) P/C50-5, (d) P/C30-5, (e) P/C60-6, (f) P/C54-6, (g) P/C39-6 and (h) P/C21-6. FE_D in red and FE_A in blue stand for Frenkel excitons locating on donor and acceptor respectively.The black dotted line represents the state where charge separation cannot occur.

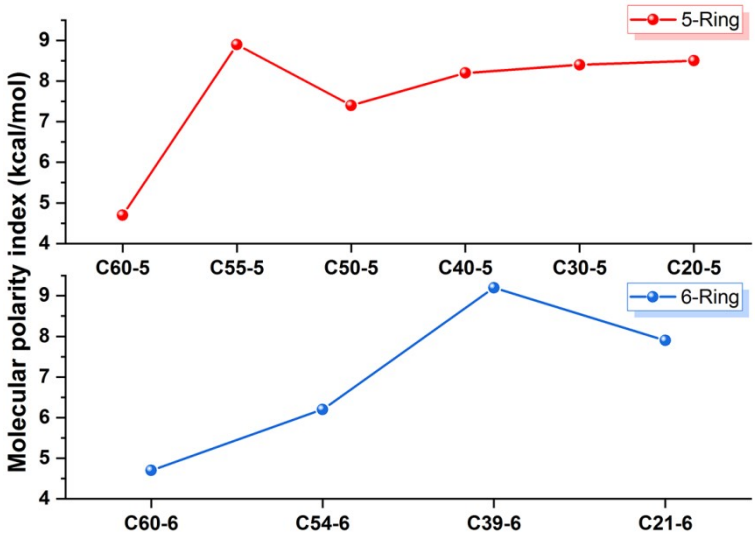

Figure S6. MPI index (kcal/mol) of fullerene and bowl-nonfullerene models including 5-ring and 6-ring models.

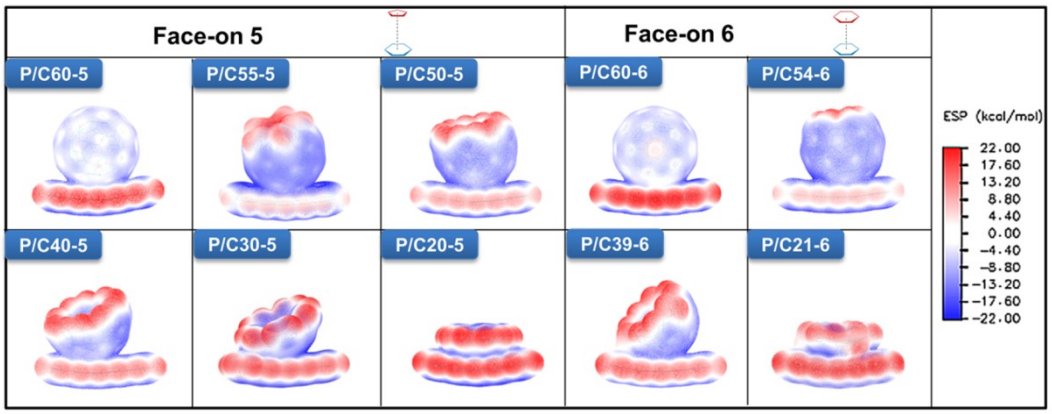

Figure S7. The electrostatic potentials (kcal/mol) of all D/A dimers in the Face-on 5 and Face-on 6 model, where red and blue denotes positive and negative value respectively.

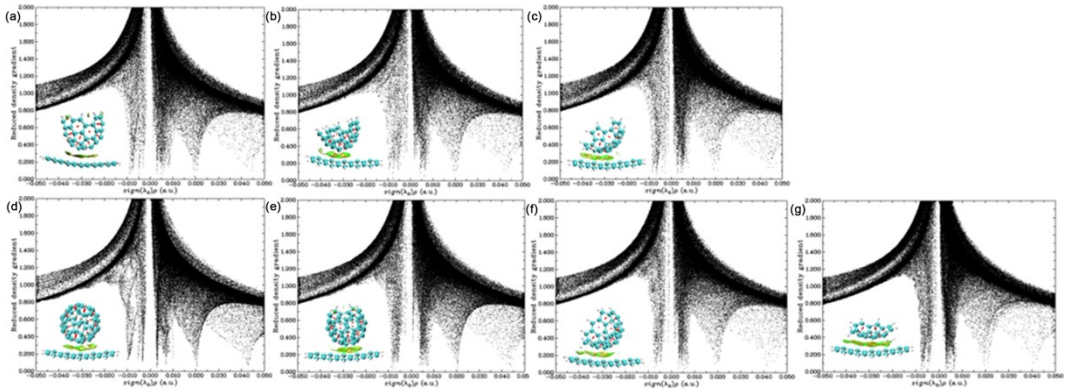

Figure S8. Scatter plots and coloring isosurface plots of sign(λ_2)ρ (a.u.) vs. RDG of other Face-on 5 and Face-on 6 models.

①The red part of isosurface graph represents steric hindrance effect between each ring,

representing 0.02~0.06 a.u in scatter diagram. ②The green and brown parts of the open ring of acceptor in isosurface map represent the bonding effect of H atoms, which is 0.0~0.01 a.u. area in scatter diagram. ③The green and brown areas between D/A in isosurface map represent weak interactions, which are -0.01~0.01 a.u in the scatter diagram.

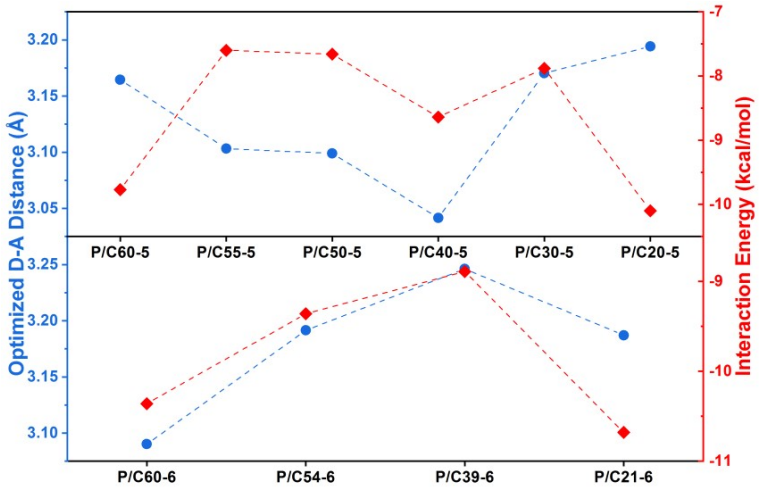

Figure S9. Interaction distance (Å) and interaction energy (kcal/mol) at the D/A interface after optimization for Face-on 5 and Face-on 6 models.

Table S2. Excitation energies (eV) and oscillator strengths (*f*) of the three lowest excited anion states of fullerene and bowl-nonfullerenes

	Excited State 1 (S_1)		Excited State 2 (S_2)		Excited State 3 (S_3)	
	Energy (eV)	*f*	Energy (eV)	*f*	Energy (eV)	*f*
$C60^-$	0.1584	0	0.1600	0	1.2162	0.0227
$C55\text{-}5^-$	0.2560	0	0.3342	0.0011	1.1444	0.0243
$C50\text{-}5^-$	0.2606	0	0.2733	0.0010	1.0796	0.0296
$C40\text{-}5^-$	1.0071	0	1.0609	0.0025	1.0610	0.0025
$C30\text{-}5^-$	0.3291	0.0001	0.3453	0.0078	1.7449	0.0006
$C20\text{-}5^-$	0.2987	0	1.8727	0.0169	1.9505	0.0622
$C54\text{-}6^-$	0.5268	0.0010	0.5271	0.0010	1.3527	0.0266
$C39\text{-}6^-$	0.2803	0.0001	0.8817	0.0049	1.5839	0.0452
$C21\text{-}6^-$	0.3774	0.0036	0.4628	0.0002	1.5739	0.0257

Notes and references

1. L.-N. Wu, M.-Y. Sui, S. Xiao, Y.-Z. Xie and G.-Y. Sun, *Phys. Chem. Chem. Phys.*, 2020, **22**, 4015-4022.
2. L.-N. Wu, M.-Y. Li, M.-Y. Sui, J.-C. Huang, G.-Y. Sun and L. Cheng, *Mater. Today Energy*, 2021, **20**, 100658.
3. P. J. Stephens, F. J. Devlin, C. F. Chabalowski and M. J. Frisch, *J. Phys. Chem.*, 1994, **98**, 11623-11627.
4. Z. L. Zheng, J.-L. Brédas and V. Coropceanu, *J. Phys. Chem. Lett.*, 2016, **7**, 2616-2621.
5. R. Baer and D. Neuhauser, *Phys. Rev. Lett.*, 2005, **94**, 043002.
6. S. Joseph, M. K. Ravva and J.-L. Bredas, *J. Phys. Chem. Lett.*, 2017, **8**, 5171-5176.
7. T Lu. optDFTω program v1.0, webpage: http://sobereva.com/346.
8. M. J. Frisch, G. E. Scuseria, M. A. Robb, J. R. Cheeseman, G. Scalmani, V. Barone, G. A. Petersson, H. Nakatsuji, X. Li, M. Caricato, A. Marenich, J. Bloino, B. G. Janesko, R.

Gomperts, B. Mennucci, H. P. Hratchian, J. V. Ortiz, A. F. Izmaylov, J. L. Sonnenberg, D. Williams-Young, F. Ding, F. Lipparini, F. Egidi, J. Goings, B. Peng, A. Petrone, T. Henderson, D. Ranasinghe, V. G. Zakrzewski, J. Gao, N. Rega, G. Zheng, W. Liang, M. Hada, M. Ehara, K. Toyota, R. Fukuda, J. Hasegawa, M. Ishida, T. Nakajima, Y. Honda, O. Kitao, H. Nakai, T. Vreven, K. Throssell, J. A. Montgomery, J. E. P. Jr., F. Ogliaro, M. Bearpark, J. J. Heyd, E. Brothers, K. N. Kudin, V. N. Staroverov, T. Keith, R. Kobayashi, J. Normand, K. Raghavachari, A. Rendell, J. C. Burant, S. S. Iyengar, J. Tomasi, M. Cossi, J. M. Millam, M. Klene, C. Adamo, R. Cammi, J. W. Ochterski, R. L. Martin, K. Morokuma, O. Farkas, J. B. Foresman and D. J. Fox, *Gaussian 09 Rev. D.01*, Wallingford, CT, 2009.

9. T. Lu and F. Chen, *J. Comput. Chem.*, 2012, **33**, 580-592.